Navier–Stokes Characteristic Boundary Conditions Using Ghost Cells

Emmanuel Motheau, Ann Almgren, John Bell

Navier-Stokes Characteristic Boundary Conditions Using Ghost Cells

Emmanuel Motheau* , Ann Almgren† and John B. Bell‡

Center for Computational Sciences and Engineering, Lawrence Berkeley National Laboratory

1 Cyclotron Rd, MS 50A-3111, Berkeley, CA 94720, USA

Solution methods for the compressible Navier-Stokes equations based on finite volume discretizations often implement boundary conditions using ghost cells outside of the computational domain. Filling the ghost cells using straightforward zeroth- or first-order extrapolation, while computationally expedient, is well-known to fail even for some simple flows, especially when turbulent structures interact with the boundaries or if time-varying inflow conditions are imposed. The Navier-Stokes Characteristic Boundary Condition (NSCBC) approach provides more accurate boundary conditions but requires the use of special discretizations at boundaries. The present paper develops a new technique based on the NSCBC approach to derive values for ghost cells that significantly improve the treatment of boundaries over simple extrapolation but retain the ghost cells approach. It is demonstrated in the context of a Godunov integration procedure that the new method provides accurate results while allowing the use of the same stencil and numerical methodology near the boundaries as in the interior.

I. Introduction

The accurate treatment of boundary conditions is critical in many computational fluid dynamics (CFD) simulations. Fundamentally, problems associated with boundary conditions for compressible flows arise because of the difficulty in ensuring a well-posed problem. This may result in the establishment of an unphysical flow in the computational domain, independent of the target values that one wants to impose. Another common problem is the generation of spurious inward-propagating waves, which again can create undesirable flow features in the domain. For example, the conversion of entropy waves to acoustic waves at

*Computational Science PostDoctoral Fellow, CCSE, Computational Research Division, EMotheau@lbl.gov
†Senior Scientist, CCSE Group Leader, Computational Research Division ASAlmgren@lbl.gov
‡Senior Scientist, Chief Scientist, Computational Research Division, JBBell@lbl.gov

the outlet of a combustion chamber may trigger a combustion instability in an aeronautical gas turbine.[1] This physical phenomenon is very sensitive to the geometry and small fluctuations of the flow, thus it is essential in numerical studies of this type of flow to accurately represent the outflow boundary conditions.

Several approaches have been proposed to derive consistent boundary conditions that would tackle the problems cited above. One of the most popular is the decomposition of the flow through 1D characteristic waves, allowing numerical control of the waves entering and leaving the domain. Initially proposed in the context of the Euler equations,[2–4] the approach has been formalized as the well-known Navier-Stokes Characteristic Boundary Conditions (NSCBC)[5] and later augmented to include viscous, reactive and three-dimensional terms.[6–11] Recent works have improved the NSCBC method to include non-linear terms[12] or to impose time domain impedances.[13]

Basically, the concept of NSCBC is to formulate an approximation of the evolution equations through the derivation of Local One-Dimensional Inviscid (LODI) relations that ensure the well-posedness of the problem. After computation of the characteristic waves crossing the boundary via the LODI relations, and possibly the addition of transverse, diffusive and reactive terms, variables are advanced to the next time step (say, from time n to $n+1$) in order to provide boundary values to compute interior points.

This procedure is particularly well adapted for finite-difference schemes or cell-vertex finite-volume methods in which fluxes are directly computed at points that lie exactly on the physical boundary of the computational domain. This kind of discretization procedure is schematically depicted in Figure 1.(a) for the finite-difference method. However, in methods such as the finite-volume Godunov method (see, e.g.[14]), time-centered fluxes at physical domain boundaries are based on extrapolation in space and time from values stored in cell centers, including, potentially, those lying outside the domain (see Figure 1.(b)). The values in ghost cells are often filled with a zeroth- or first-order extrapolation method. Whereas this technique provides good results for one-dimensional simulations of the Euler equations as it corresponds to a well-posed problem, the application to complex multi-dimensional flows leads to significant errors, with spurious unphysical waves generated that propagate back into the computational domain.[5,14] As a remedy, filtering techniques via the imposition of an artificial field near boundaries have been proposed,[15–17] but their efficiency in practical applications is questionable.

Application of the characteristic boundary condition strategy in the context of methods using ghost cells methods is problematic. For example in the context of the finite-volume Godunov procedure, a direct implementation as proposed in the references aforementioned would require special discretizations at physical boundaries. To the author's knowledge, only one paper[18] has been published in the literature to deal with characteristic ghost cells boundary conditions. However this work proposes only a first-order technique to fill a single ghost cell in one dimension. There is also no discussion about the implementation of transverse

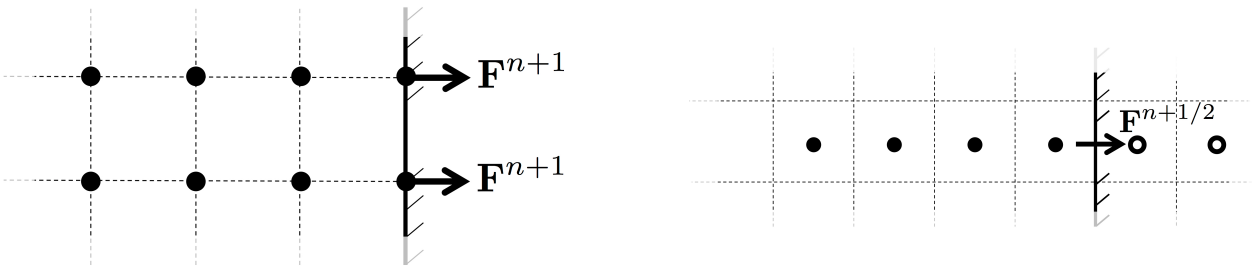

(a) (b)

Figure 1. Schematic representation of examples of discretization procedures of the flux F for the finite-difference method (a) and the finite-volume Godunov method (b).

terms or how to deal with ghost cells around corners in multi-dimensional domains.

The aim of the present paper is to present a generic multi-dimensional approach for imposing Navier-Stokes Characteristic Boundary Conditions in numerical methods that use multiple ghost cells. It will be referred to as the GC-NSCBC approach. While the method is described here in the context of a Godunov integration procedure, it is applicable to other integration schemes that use ghost cells. For ease of exposition, the method is presented in two dimensions, but extension to three dimensions is straightforward. In addition, the treatment of transverse terms as well as corners for different sets of mixed-conditions in two dimensions will be described. Results computed using this approach will be further compared with examples in the current literature.

II. Governing equations

The fully compressible Navier-Stokes equations in two-dimensional Cartesian coordinates are expressed as

$$\frac{\partial \mathbf{U}}{\partial t} + \frac{\partial \mathbf{F}_c}{\partial x} + \frac{\partial \mathbf{G}_c}{\partial y} = \mathbf{S}_v. \tag{1}$$

In Eq. (1), subscripts c and v refer to the convective and viscous terms, respectively. Here $\mathbf{U}$ is the conserved state vector

$$\mathbf{U} = \begin{pmatrix} \rho \\ \rho u \\ \rho v \\ \rho E \end{pmatrix}, \tag{2}$$

and the inviscid convective flux vectors are given as

$$\mathbf{F}_c = \begin{pmatrix} \rho u \\ \rho u^2 + p \\ \rho v u \\ (\rho E + p)\, u \end{pmatrix}, \qquad \mathbf{G}_c = \begin{pmatrix} \rho v \\ \rho u v \\ \rho v^2 + p \\ (\rho E + p)\, v \end{pmatrix}. \tag{3}$$

The source term $\mathbf{S}_v$ contains derivatives of the viscous fluxes

$$\mathbf{S}_v = \frac{\partial \mathbf{F}_v}{\partial x} + \frac{\partial \mathbf{G}_v}{\partial y}, \tag{4}$$

where

$$\mathbf{F}_v = \begin{pmatrix} 0 \\ \tau_{xx} \\ \tau_{xy} \\ \tau_{xx} u + \tau_{xy} v + \lambda \frac{\partial T}{\partial x} \end{pmatrix}, \qquad \mathbf{G}_v = \begin{pmatrix} 0 \\ \tau_{yx} \\ \tau_{yy} \\ \tau_{yx} u + \tau_{yy} v + \lambda \frac{\partial T}{\partial y} \end{pmatrix}. \tag{5}$$

Here, ρ is the fluid mass density whereas u and v are the velocity components in the x- and y-directions, respectively. The total energy per unit mass is expressed as $E = e + (u^2 + v^2)/2$, where e is the specific internal energy. The thermodynamic pressure p is related to the energy through the following equation of state for an ideal single-component gas:

$$p = (\gamma - 1)\, \rho e = \rho \mathcal{R} T, \tag{6}$$

where T is the temperature, $\mathcal{R}$ the gas constant and γ the ratio of the specific heats. The components of the viscous stress tensor τ are given by

$$\tau_{xx} = 2\mu \frac{\partial u}{\partial x} - \frac{2}{3}\mu \left(\frac{\partial u}{\partial x} + \frac{\partial v}{\partial y} \right), \tag{7}$$

$$\tau_{yy} = 2\mu \frac{\partial v}{\partial y} - \frac{2}{3}\mu \left(\frac{\partial u}{\partial x} + \frac{\partial v}{\partial y} \right), \tag{8}$$

$$\tau_{xy} = \tau_{yx} = \mu \left(\frac{\partial v}{\partial x} + \frac{\partial u}{\partial y} \right), \tag{9}$$

where the viscosity coefficient μ is obtained from the thermal conductivity λ according to

$$\lambda = \mu C_p / Pr, \tag{10}$$

with Pr the Prandtl number and C_p the specific heat capacity at constant pressure.

III. Integration Algorithm

While the GC-NSCBC method is applicable to a variety of integration schemes, for ease of exposition and concreteness of examples it will presented in the context of a second-order conservative finite-volume unsplit Godunov method. All numerical results are computed using the implementation of the algorithm in **CASTRO**,[19] a compressible flow solver based on BoxLib,[20,21] a hybrid C++ /Fortran90 software framework that provides support for the development of parallel structured-grid AMR applications.

The solution is advanced from time n to time $n+1$ as follows:

$$\mathbf{U}^* = \mathbf{U}^n - \Delta t \left(\frac{\partial \mathbf{F}_c}{\partial x} + \frac{\partial \mathbf{G}_c}{\partial y} \right)^{n+1/2} + \Delta t \; \mathbf{S}_v^n, \tag{11}$$

$$\mathbf{U}^{n+1} = \mathbf{U}^* + \frac{1}{2}\Delta t \left(\mathbf{S}_v^* - \mathbf{S}_v^n \right). \tag{12}$$

where $\Delta t = t^{n+1} - t^n$ is the time step. The second step at Eq. (12) is a correction of the solution to ensure second-order accuracy by effectively time-centering the diffusion source terms.

The conserved state vector $\mathbf{U}$ is stored at cell centers and the flux vectors, $\mathbf{F}_{c,v}$ and $\mathbf{G}_{c,v}$, are computed on cell edges. Recall that here, subscripts c and v refer to either the convective or viscous terms, respectively. The gradients of fluxes are simply discretized using centered finite differences:

$$\left. \frac{\partial \mathbf{F}_{c,v}}{\partial x} \right|_{i,j} = \frac{(\mathbf{F}_{c,v})_{i+\frac{1}{2},j} - (\mathbf{F}_{c,v})_{i-\frac{1}{2},j}}{\Delta x}, \tag{13}$$

$$\left. \frac{\partial \mathbf{G}_{c,v}}{\partial y} \right|_{i,j} = \frac{(\mathbf{G}_{c,v})_{i,j+\frac{1}{2}} - (\mathbf{G}_{c,v})_{i,j-\frac{1}{2}}}{\Delta y}, \tag{14}$$

with the viscous flux vectors discretized as follows:

$$(\mathbf{F}_v)_{i+\frac{1}{2},j} = \begin{pmatrix} 0 \\ \frac{4}{3\Delta x}\mu \left(u_{i+1,j} - u_{i,j}\right) - \frac{1}{6\Delta y}\mu \left[\left(v_{i+1,j+1} - v_{i+1,j-1}\right) + \left(v_{i,j+1} - v_{i,j-1}\right) \right] \\ \frac{1}{4\Delta y}\mu \left[\left(u_{i+1,j+1} - u_{i+1,j-1}\right) + \left(u_{i,j+1} - u_{i,j-1}\right) \right] + \frac{1}{\Delta x}\mu \left(v_{i+1,j} - v_{i,j}\right) \\ \frac{1}{2}\left(u_{i+1,j} + u_{i,j}\right)\left(\mathbf{F}_{v,2}\right)_{i+\frac{1}{2},j} + \frac{1}{2}\left(v_{i+1,j} + v_{i,j}\right)\left(\mathbf{F}_{v,3}\right)_{i+\frac{1}{2},j} + \frac{1}{\Delta x}\lambda \left(T_{i+1,j} - T_{i,j}\right) \end{pmatrix}, \tag{15}$$

$$(\mathbf{G}_v)_{i,j+\frac{1}{2}} = \begin{pmatrix} 0 \\ \frac{1}{4\Delta x}\mu \left[\left(v_{i+1,j+1} - v_{i-1,j+1}\right) + \left(v_{i+1,j} - v_{i-1,j}\right) \right] + \frac{1}{\Delta y}\mu \left(u_{i,j+1} - u_{i,j}\right) \\ \frac{4}{3\Delta x}\mu \left(v_{i,j+1} - v_{i,j}\right) - \frac{1}{6\Delta y}\mu \left[\left(u_{i+1,j+1} - u_{i-1,j+1}\right) + \left(u_{i+1,j} - u_{i-1,j}\right) \right] \\ \frac{1}{2}\left(u_{i,j+1} + u_{i,j}\right)\left(\mathbf{G}_{v,2}\right)_{i,j+\frac{1}{2}} + \frac{1}{2}\left(v_{i,j+1} + v_{i,j}\right)\left(\mathbf{G}_{v,3}\right)_{i,j+\frac{1}{2}} + \frac{1}{\Delta y}\lambda \left(T_{i,j+1} - T_{i,j}\right) \end{pmatrix}. \tag{16}$$

where $\mathbf{F}_{v,m}$ and $\mathbf{G}_{v,m}$, $m = 1, \ldots, 4$, represent the components of the discrete viscous flux vectors in Eqs. (15) and (16), respectively.

The convective flux vectors $\mathbf{F}_c$ and $\mathbf{G}_c$ that appear in Eq. (11) are constructed from time-centered edge states computed with a conservative, shock-capturing, unsplit Godunov method, which makes use of the Piecewise Parabolic Method (PPM), characteristic tracing and full corner coupling.[19,22,23] The integration procedure is complex and a complete description is out of scope of the present paper. It will only be summarized below and details can be found in the aforementioned references. Basically this particular procedure follows four major steps:

1. The conservative Eq. (1) is rewritten in terms of primitive variables, such that:

$$\frac{\partial \mathbf{Q}}{\partial t} + \widetilde{\mathbf{F}} \frac{\partial \mathbf{Q}}{\partial x} + \widetilde{\mathbf{G}} \frac{\partial \mathbf{Q}}{\partial y} = \mathbf{S}_{\mathbf{Q}}. \tag{17}$$

   Here $\mathbf{Q} = \{\rho, u, v, p\}$ is the primitive state vector, whereas $\widetilde{\mathbf{F}}$ and $\widetilde{\mathbf{G}}$ are the non-conservative Jacobian matrices defined as

$$\widetilde{\mathbf{F}} = \begin{pmatrix} u & \rho & 0 & 0 \\ 0 & u & 0 & \frac{1}{\rho} \\ 0 & 0 & u & 0 \\ 0 & \rho c^2 & 0 & u \end{pmatrix}, \qquad \widetilde{\mathbf{G}} = \begin{pmatrix} v & 0 & \rho & 0 \\ 0 & v & 0 & 0 \\ 0 & 0 & v & \frac{1}{\rho} \\ 0 & 0 & \rho c^2 & v \end{pmatrix}. \tag{18}$$

   where $c = \sqrt{\gamma p/\rho}$ is the sound speed, and the viscous source terms $\mathbf{S}_{\mathbf{Q}}$ are given by

$$\mathbf{S}_{\mathbf{Q}} = \frac{\partial}{\partial x} \begin{pmatrix} 0 \\ \frac{1}{\rho}\mathbf{F}_{v,2} \\ \frac{1}{\rho}\mathbf{F}_{v,3} \\ (\gamma - 1)\,\mathbf{F}_{v,4} \end{pmatrix} + \frac{\partial}{\partial y} \begin{pmatrix} 0 \\ \frac{1}{\rho}\mathbf{G}_{v,2} \\ \frac{1}{\rho}\mathbf{G}_{v,3} \\ (\gamma - 1)\,\mathbf{G}_{v,4} \end{pmatrix}. \tag{19}$$

2. A piecewise quadratic parabolic profile approximation of $\mathbf{Q}$ is constructed within each cell with a modified version of the PPM algorithm.[19] These constructions are performed in each coordinate direction separately.

3. Average values of $\mathbf{Q}$ are predicted on edges over the time step using characteristic extrapolation. A characteristic tracing operator with flattening is applied to the integrated quadratic profiles in order to obtain left and right edge states at time $n + 1/2$.

4. The time-centered fluxes are computed using an approximate Riemann problem solver. At the end of this procedure the primitive variables are centered in time at $n+1/2$, and in space on the edges of a cell. This is the so-called *Godunov state* and the convective fluxes described at Eq. (5) can be computed to advance Eq. (11).

IV. Navier-Stokes Characteristic Boundary Conditions

In this section a methodology based on the NSCBC approach is presented to determine the values of primitive variables stored at the centers of the ghost cells. The discretization described in Sec. III employs a spatial stencil composed of 9 points in each coordinate direction. The PPM integration strategy requires information from 4 cells in each positive and negative coordinate direction, thus 4 ghost cells are required. A piecewise linear approach with 4th order slopes, for example, would require 3 ghost cells, but the GC-NSCBC methodology would be identical; it is emphasized that this approach works for an arbitrary number of ghost cells and a variety of integration strategies.

IV.A. Characteristic formulation in one dimension for edges

Eq. (17) can be reformulated in terms of characteristic waves traveling along the axis x through the diagonalization of the vector $\widetilde{\mathbf{F}}$:

$$\frac{\partial \mathbf{Q}}{\partial t} + \mathbf{S}_{(x)} \mathbf{\Lambda} \mathbf{S}_{(x)}^{-1} \frac{\partial \mathbf{Q}}{\partial x} + \widetilde{\mathbf{G}} \frac{\partial \mathbf{Q}}{\partial y} = \mathbf{S}_{\mathbf{Q}}, \tag{20}$$

where $\mathbf{\Lambda} = \lambda \mathbf{I}_4$ is a diagonal matrix containing the eigenvalues, which physically represents the propagation speeds of the characteristic waves:

$$\lambda_1 = u - c, \quad \lambda_{2,3} = u, \quad \lambda_4 = u + c. \tag{21}$$

The eigenvector matrix $\mathbf{S}_{(x)}$ and its inverse $\mathbf{S}_{(x)}^{-1}$ are defined as

$$\mathbf{S}_{(x)} = \begin{pmatrix} \frac{1}{2c^2} & \frac{1}{c^2} & 0 & \frac{1}{2c^2} \\ -\frac{1}{2\rho c} & 0 & 0 & \frac{1}{2\rho c} \\ 0 & 0 & 1 & 0 \\ \frac{1}{2} & 0 & 0 & \frac{1}{2} \end{pmatrix}, \qquad \mathbf{S}_{(x)}^{-1} = \begin{pmatrix} 0 & -\rho c & 0 & 1 \\ c^2 & 0 & 0 & -1 \\ 0 & 0 & 1 & 0 \\ 0 & \rho c & 0 & 1 \end{pmatrix}. \tag{22}$$

A vector $\mathcal{L}$ containing the amplitude time variations of the characteristic waves[5] is defined as

$$\mathcal{L} = \mathbf{\Lambda}\mathbf{S}_{(x)}^{-1}\frac{\partial \mathbf{Q}}{\partial x} = \begin{pmatrix} \lambda_1\left(\frac{\partial p}{\partial x} - \rho c\frac{\partial u}{\partial x}\right) \\ \lambda_2\left(c^2\frac{\partial \rho}{\partial x} - \frac{\partial p}{\partial x}\right) \\ \lambda_3\frac{\partial v}{\partial x} \\ \lambda_4\left(\frac{\partial p}{\partial x} + \rho c\frac{\partial u}{\partial x}\right) \end{pmatrix}. \tag{23}$$

Eq. (23) is then put back into Eq. (20), leading to:

$$\frac{\partial \mathbf{Q}}{\partial t} + \mathbf{d} + \widetilde{\mathbf{G}}\frac{\partial \mathbf{Q}}{\partial y} = \mathbf{S}_{\mathbf{Q}}, \tag{24}$$

where $\mathbf{d}$ is the so-called LODI system[5] and is expressed as

$$\mathbf{d} = \mathbf{S}_{(x)}\mathcal{L} = \begin{pmatrix} \frac{1}{c^2}\left[\mathcal{L}_2 + \frac{1}{2}\left(\mathcal{L}_4 + \mathcal{L}_1\right)\right] \\ \frac{1}{2\rho c}\left(\mathcal{L}_4 - \mathcal{L}_1\right) \\ \mathcal{L}_3 \\ \frac{1}{2}\left(\mathcal{L}_4 + \mathcal{L}_1\right) \end{pmatrix}. \tag{25}$$

Eq. (23) can be discretized to compute *in a strong way* the amplitude of the time variations of the characteristic waves. In contrast, the principle of the NSCBC approach is to provide a model for the expressions in Eq. (23) so as to impose *in a soft way* the desired physical properties at the boundary. In practice, waves leaving the domain are numerically computed from interior values while incoming waves are imposed via analytical expressions aiming to introduce a damping behavior. However, the underlying assumption is that the flow at the boundary is considered to be locally inviscid and one-dimensional, and this may lead to unphysical results for complex multi-dimensional flows. As explained in the introduction, there is a large literature investigating how to introduce properly transverse, viscous and reactive effects in the expression of $\mathcal{L}$.

In most applications, Eq. (24) is employed to predict the solution vector $\mathbf{Q}$ at time $n+1$ at the physical boundary of the computational domain. In the Godunov procedure described here, ghost cells values must be expressed at time n and the time-derivative in Eq. (24) vanishes. The main idea of the present method is to express the spatial derivative in the last interior cell of the computational domain so as to provide an expression for the ghost cells with the help of finite-difference schemes. This can be easily done by applying a backward transformation to Eq. (23), leading to:

$$\frac{\partial \mathbf{Q}}{\partial x} = \mathbf{S}_{(x)}\mathbf{\Lambda}^{-1}\mathcal{L}. \tag{26}$$

If one defines a domain of length l_x discretized along the x axis by a uniform distribution of $i = 1, \ldots, L_x$ points, the values of $\mathbf{Q}$ at the center of the ghost cells outside of the left boundary at $i = 1$ are defined by

$$\mathbf{Q}_{i-1} = \mathbf{Q}_{i+1} - 2\Delta x \frac{\partial \mathbf{Q}}{\partial x}, \tag{27}$$

$$\mathbf{Q}_{i-2} = -2\mathbf{Q}_{i+1} - 3\mathbf{Q}_i + 6\mathbf{Q}_{i-1} + 6\Delta x \frac{\partial \mathbf{Q}}{\partial x}, \tag{28}$$

$$\mathbf{Q}_{i-3} = 3\mathbf{Q}_{i+1} + 10\mathbf{Q}_i - 18\mathbf{Q}_{i-1} + 6\mathbf{Q}_{i-2} - 12\Delta x \frac{\partial \mathbf{Q}}{\partial x}, \tag{29}$$

$$\mathbf{Q}_{i-4} = -2\mathbf{Q}_{i+1} - 13\mathbf{Q}_i + 24\mathbf{Q}_{i-1} - 12\mathbf{Q}_{i-2} + 4\mathbf{Q}_{i-3} + 12\Delta x \frac{\partial \mathbf{Q}}{\partial x}. \tag{30}$$

Similarly, the values of $\mathbf{Q}$ in the points located in the ghost cells outside of the right boundary at $i = L_x$ are defined by

$$\mathbf{Q}_{i+1} = \mathbf{Q}_{i-1} + 2\Delta x \frac{\partial \mathbf{Q}}{\partial x}, \tag{31}$$

$$\mathbf{Q}_{i+2} = -2\mathbf{Q}_{i-1} - 3\mathbf{Q}_i + 6\mathbf{Q}_{i+1} - 6\Delta x \frac{\partial \mathbf{Q}}{\partial x}, \tag{32}$$

$$\mathbf{Q}_{i+3} = 3\mathbf{Q}_{i-1} + 10\mathbf{Q}_i - 18\mathbf{Q}_{i+1} + 6\mathbf{Q}_{i+2} + 12\Delta x \frac{\partial \mathbf{Q}}{\partial x}, \tag{33}$$

$$\mathbf{Q}_{i+4} = -2\mathbf{Q}_{i-1} - 13\mathbf{Q}_i + 24\mathbf{Q}_{i+1} - 12\mathbf{Q}_{i+2} + 4\mathbf{Q}_{i+3} - 12\Delta x \frac{\partial \mathbf{Q}}{\partial x}. \tag{34}$$

Note that here the index j has been omitted for clarity. Ghost cells at the top and bottom boundaries could be filled analogously.

IV.A.1. Subsonic non-reflecting outflow

Let us consider an outflow boundary condition at one edge of a 2D Cartesian domain. In this case, only one unknown wave is entering the domain and its amplitude variation is modeled as

$$\mathcal{L}_\phi = K\left(p - p_t\right) - \left(1 - \beta\right)\mathcal{T}_\phi, \tag{35}$$

where $\phi = 1$ or $\phi = 4$ if the boundary is located at $i = L_x$ or $i = 1$, respectively. The term p_t refers to a target pressure that one wants to impose at the outflow, and β is a parameter to control the amount of contribution of the transverse term $\mathcal{T}_\phi$ defined either as

$$\mathcal{T}_1 = v\left(\frac{\partial p}{\partial y} - \rho c \frac{\partial u}{\partial y}\right) + \gamma p \frac{\partial v}{\partial y}, \tag{36}$$

or

$$\mathcal{T}_4 = v\left(\frac{\partial p}{\partial y} + \rho c \frac{\partial u}{\partial y}\right) + \gamma p \frac{\partial v}{\partial y}. \tag{37}$$

Finally, the term K is a relaxation coefficient parameter defined by

$$K = \sigma c \left(1 - M^2\right) / l_x, \tag{38}$$

with σ a constant parameter usually set to 0.25.

It is worth noting that the choice of the parameters σ and β is highly dependent on the physics of the flow. Moreover, the Mach number M may be taken locally or averaged over the whole surface where the outflow boundary is imposed. Many studies have investigated the impact of these parameters to minimize spurious reflections when multi-dimensional vortical structures are leaving the domain,[5,7–11,24] and there has yet to be a consensus on a generic choice.

The remaining waves are computed according to Eq. (23). The spatial derivatives are evaluated from known interior points with a second-order one-sided finite difference scheme. If one defines first a generic variable Υ that may be either ρ, u, v or p, the spatial derivative of Υ is expressed as follows for a boundary located at

- $i = 1$:

$$\frac{\partial \Upsilon}{\partial x} = \frac{-3\Upsilon_i + 4\Upsilon_{i+1} - 1\Upsilon_{i+2}}{2\Delta x}, \tag{39}$$

- $i = L_x$:

$$\frac{\partial \Upsilon}{\partial x} = \frac{\Upsilon_{i-2} - 4\Upsilon_{i-1} + 3\Upsilon_i}{2\Delta x}. \tag{40}$$

Again, note that here the index j has been omitted for clarity as the derivatives are computed for all j.

Similarly, the spatial derivatives that appear in the transverse terms described in Eq. (36) and (37) are evaluated with a second-order central finite-difference scheme:

$$\frac{\partial \Upsilon}{\partial y} = \frac{\Upsilon_{i,j+1} - \Upsilon_{i,j-1}}{2\Delta y}, \tag{41}$$

where here i is either 1 or L_x depending on the location of the boundary. Note that for the very first or last ghost cells in the y direction, and if no periodicity conditions are involved, Eq. (41) degenerates to a one-sided scheme similar to Eq. (39) or Eq. (40).

IV.A.2. Subsonic non-reflecting inflow

For a subsonic non-reflecting inflow, three waves are entering the domain while only one is leaving. The amplitude variations with transverse terms are imposed in a soft way as follows:[8]

$$\mathcal{L}_\phi = \eta_\phi \frac{\rho c^2 \left(1 - M^2\right)}{l_x} \left(u - u_t\right) - \mathcal{T}_\phi \tag{42}$$

$$\mathcal{L}_2 = \eta_2 \frac{\rho c \mathcal{R}}{l_x} \left(T - T_t\right) - \mathcal{T}_2 \tag{43}$$

$$\mathcal{L}_3 = \eta_3 \frac{c}{l_x} \left(v - v_t\right) - \mathcal{T}_3 \tag{44}$$

where η are parameters controlling the damping of the amplitude of waves imposed to the domain, while the index t refers to target values of the primitive variables. Again, $\phi = 1$ or $\phi = 4$ if the boundary is located at $i = L_x$ or $i = 1$, respectively, and the corresponding transverse terms $\mathcal{T}_\phi$ are defined at Eqs. (36) and (37). The remaining transverse terms are given by

$$\mathcal{T}_2 = v \left(c^2 \frac{\partial \rho}{\partial y} - \frac{\partial p}{\partial y} \right) + c^2 \rho \frac{\partial v}{\partial y} - \gamma p \frac{\partial v}{\partial y} \tag{45}$$

$$\mathcal{T}_3 = v \frac{\partial v}{\partial y} + \frac{1}{\rho} \frac{\partial p}{\partial y} \tag{46}$$

IV.A.3. Adiabatic/isothermal viscous/slip walls

In the case of viscous or slip walls, the velocity normal to a boundary is zero. Thus, waves $\mathcal{L}_2$ and $\mathcal{L}_3$ vanish. Moreover, as the time derivative of the velocity in Eq. (24) also vanishes, it implies that $\mathcal{L}_1 = \mathcal{L}_4$. To be consistent with the inflow/outflow conditions, $\phi = 1$ or $\phi = 4$ if the boundary is located at $i = L_x$ or $i = 1$, respectively. Thus, after defining $\phi^* = 5 - \phi$, the wave $\mathcal{L}_{\phi^*}$ impacting the wall in the normal direction is computed numerically from interior points, and $\mathcal{L}_\phi$ is set to $\mathcal{L}_{\phi^*}$.

In the present paper, viscous and slip walls are treated in the same manner during the computation of the waves $\mathcal{L}$. Once the convective fluxes have been computed through the Godunov procedure, GC-NSCBC values are no longer needed, and velocity and temperature values are enforced in ghost cells during the computation of the viscous fluxes. Recall that for a viscous wall, both u and v are set to zero, while for a slip wall only the velocity in the normal direction vanishes. Note that a different formulation of the waves has been proposed[9] to take into account viscous terms at this stage. This approach has not been tested in the present work but its implementation is straightforward in the context of GC-NSCBC. Beside the treatment of velocities at walls, the procedure is rather similar for the diffusive heat fluxes. If adiabatic walls are considered, the temperature in the ghost cells is computed from the last interior node with a zeroth-order extrapolation technique so a to reproduce a zero heat flux. For isothermal walls, the desired temperature is

imposed straight inside the ghost cells.

IV.B. Characteristic formulation in two dimensions for corners

In a 2D Cartesian square domain, corners require a particular treatment because characteristic waves in both the $x-$ and $y-$directions are coupled. Depending on the physical boundary conditions, a linear system in the unknown waves has to be solved. Moreover, when the corner shares boundaries of different type, an additional compatibility condition must be introduced to ensure numerical stability. These issues have been investigated in details by Lodato *et al.*[10] for 2D and 3D configurations. The present paper aims to revisit the corner treatment proposed in this latter reference, but in the context of the ghost cells implementation.

At a corner, Eq. (17) is reformulated in terms of characteristic waves traveling along the axis x and y through the diagonalization of the vector $\widetilde{\mathbf{F}}$ and $\widetilde{\mathbf{G}}$ as follows:

$$\frac{\partial \mathbf{Q}}{\partial t} + \mathbf{S}_{(x)}\mathbf{\Lambda}\mathbf{S}_{(x)}^{-1}\frac{\partial \mathbf{Q}}{\partial x} + \mathbf{S}_{(y)}\mathbf{M}\mathbf{S}_{(y)}^{-1}\frac{\partial \mathbf{Q}}{\partial y} = \mathbf{S}_{\mathbf{Q}}, \tag{47}$$

where $\mathbf{\Lambda} = \lambda \mathbf{I}_4$ and $\mathbf{M} = \xi \mathbf{I}_4$ are diagonal matrix containing the eigenvalues of $\widetilde{\mathbf{F}}$ and $\widetilde{\mathbf{G}}$, respectively, with

$$\lambda_1 = u - c, \;\; \lambda_{2,3} = u, \;\; \lambda_4 = u + c, \tag{48}$$

$$\xi_1 = v - c, \;\; \xi_{2,3} = v, \;\; \xi_4 = v + c. \tag{49}$$

Here, the eigenvector matrix $\mathbf{S}_{(y)}$ and its inverse $\mathbf{S}_{(y)}^{-1}$ are defined as

$$\mathbf{S}_{(y)} = \begin{pmatrix} \frac{1}{2c^2} & 0 & \frac{1}{c^2} & \frac{1}{2c^2} \\ 0 & 1 & 0 & 0 \\ -\frac{1}{2\rho c} & 0 & 0 & \frac{1}{2\rho c} \\ \frac{1}{2} & 0 & 0 & \frac{1}{2} \end{pmatrix}, \qquad \mathbf{S}_{(y)}^{-1} = \begin{pmatrix} 0 & 0 & -\rho c & 1 \\ 0 & 1 & 0 & 0 \\ c^2 & 0 & 0 & -1 \\ 0 & 0 & \rho c & 1 \end{pmatrix}. \tag{50}$$

The wave amplitude time variations are defined as

$$\mathcal{L} = \mathbf{\Lambda}\mathbf{S}_{(x)}^{-1}\frac{\partial \mathbf{Q}}{\partial x}, \tag{51}$$

$$\mathcal{M} = \mathbf{M}\mathbf{S}_{(y)}^{-1}\frac{\partial \mathbf{Q}}{\partial y}, \tag{52}$$

where $\mathcal{L}$ is expressed by Eq. (23) and $\mathcal{M}$ is

$$\mathcal{M} = \begin{pmatrix} \xi_1 \left(\frac{\partial p}{\partial y} - \rho c \frac{\partial v}{\partial y} \right) \\ \xi_2 \frac{\partial u}{\partial y} \\ \xi_3 \left(c^2 \frac{\partial \rho}{\partial y} - \frac{\partial p}{\partial y} \right) \\ \xi_4 \left(\frac{\partial p}{\partial y} + \rho c \frac{\partial v}{\partial y} \right) \end{pmatrix}. \tag{53}$$

Finally, in a similar way that in Sec. IV.A, the spatial derivatives of the primitive variables at the corner point are defined as

$$\frac{\partial \mathbf{Q}}{\partial x} = \mathbf{S}_{(x)} \mathbf{\Lambda}^{-1} \mathcal{L}, \tag{54}$$

$$\frac{\partial \mathbf{Q}}{\partial y} = \mathbf{S}_{(y)} \mathbf{M}^{-1} \mathcal{M}. \tag{55}$$

The procedure to compute ghost cells is depicted in Figure 2 and consists of 2 steps:

1. Once the wave amplitude time variations $\mathcal{L}$ and $\mathcal{M}$ are computed, the spatial derivatives expressed at Eqs. (54)-(55) are employed together with Eqs. (27)-(34) to fill the ghost cells in the $x-$ and $y-$axis of $\mathbf{Q}_{i,j}$, where i can be either 1 or L_x, and j either 1 or L_y.

2. The remaining ghost cells for each boundary edge are treated as in Sec. IV.A.

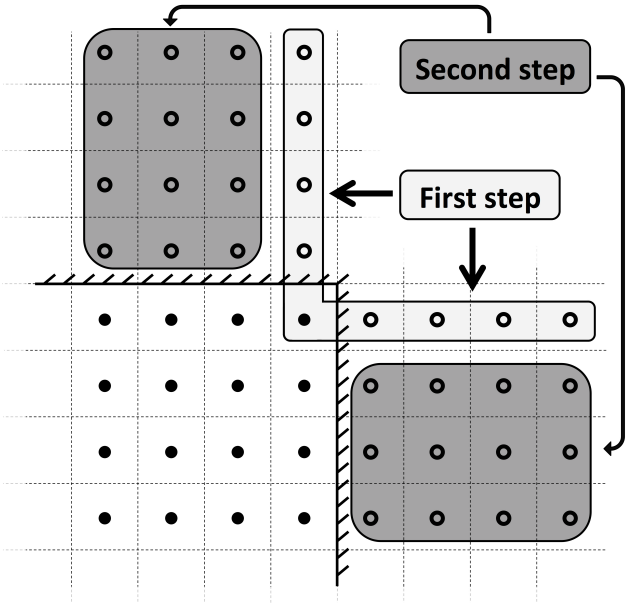

Figure 2. Schematic representation of the treatment procedure for computation of ghost cells around corners.

IV.B.1. Outflow/outflow corner

The system of unknown waves are solutions of the system:[10]

$$\begin{cases} \mathcal{L}_\phi + \dfrac{1-\beta}{2}\mathcal{M}_\psi & = \sigma\dfrac{c\left(1-M^2\right)}{L_x}\left(p-p_t\right) - \left(1-\beta\right)\left(\dfrac{\mathcal{M}_{\psi^*}}{2} + \zeta\left(\phi\right)\rho c\mathcal{M}_2\right) \\ \dfrac{1-\beta}{2}\mathcal{L}_\phi + \mathcal{M}_\psi & = \sigma\dfrac{c\left(1-M^2\right)}{L_y}\left(p-p_t\right) - \left(1-\beta\right)\left(\dfrac{\mathcal{L}_{\phi^*}}{2} + \zeta\left(\psi\right)\rho c\mathcal{L}_3\right) \end{cases} \tag{56}$$

Here the wave amplitude time variations $\mathcal{L}$ and $\mathcal{M}$ are identified by indexes ϕ and ψ, depending on their location in the computational domain. Table 1 summarizes all possible configurations. Similarly as in Sec. IV.A.3, $\phi^* = 5 - \phi$ and $\psi^* = 5 - \psi$. The term ζ is a switch defined as

$$\zeta\left(\phi\right) = \frac{\phi - 1}{2} = \begin{cases} -1 & \text{if } \phi = 1 \\ +1 & \text{if } \phi = 4 \end{cases} \tag{57}$$

As recalled by Lodato *et al.*,[10] the system (56) always admits a solution for $0 \leqslant \beta \leqslant 1$.

	ϕ	ψ	ϕ	ψ
i / j	1		L_x	
1	4	4	1	4
L_y	4	1	1	1

Table 1. Indices ϕ and ψ identifying waves $\mathcal{L}$ and $\mathcal{M}$ depending on the edge location.

IV.B.2. Inflow/outflow corner

The treatment of a corner sharing inflow and outflow boundary edges is more problematic. In principle, all the waves for both boundary edges could be imposed, but it would lead to numerical instability. In practice, a so-called *compatibility condition* is set to relax the boundary conditions.[5] In the present case, the incoming wave amplitude relative to the outflow boundary condition is set to zero so that the pressure is then free to adapt to the local flow field.[10]

As an example, let us define the inflow and outflow boundary conditions normal to the $x-$ and $y-$direction,

respectively. The unknown waves are then expressed as

$$\mathcal{M}_\psi = 0 \quad \text{(compatibility condition)} \tag{58}$$

$$\mathcal{L}_\phi = \eta_\phi \frac{\rho c^2 \left(1 - M^2\right)}{l_x} \left(u - u_t\right) - \frac{\mathcal{M}_{\psi^*}}{2} - \zeta\left(\phi\right) \rho c \mathcal{M}_2 \tag{59}$$

$$\mathcal{L}_2 = \eta_2 \frac{\rho c \mathcal{R}}{l_x} \left(T - T_t\right) - \mathcal{M}_3 \tag{60}$$

$$\mathcal{L}_3 = \eta_3 \frac{c}{l_x} \left(v - v_t\right) + \frac{\zeta\left(\psi\right)}{2\rho c} \mathcal{M}_{\psi^*} \tag{61}$$

Again, the indices ϕ and ψ and the value of ζ are obtained from Table. 1 and Eq. (57).

IV.B.3. Wall/outflow corner

In this case, the wall boundary edge is treated without any other assumption as in Sec. IV.A.3, and the known acoustic wave is introduced as a transverse term in the computation of the outgoing wave relative to the outflow direction. If one sets the outflow and wall boundary conditions normal to the $x-$ and $y-$direction, the system of unknown waves is then

$$\mathcal{M}_\psi = \mathcal{M}_{\psi^*} \tag{62}$$

$$\mathcal{L}_\phi = K\left(p - p_t\right) - \left(1 - \beta\right) \mathcal{M}_{\phi^*} \tag{63}$$

with K defined at Eq. (38).

IV.B.4. Wall/inflow edges

Let us consider the configuration where the inflow is on the $x-$direction and a wall is normal to the $y-$direction. Following the discussion presented at Sec. IV.B.2 and IV.B.3, the system of unknown waves is then expressed as

$$\mathcal{M}_\psi = \mathcal{M}_{\psi^*} \tag{64}$$

$$\mathcal{L}_\phi = \eta_\phi \frac{\rho c^2 \left(1 - M^2\right)}{l_x} \left(u - u_t\right) - \frac{\mathcal{M}_{\psi^*}}{2} \tag{65}$$

$$\mathcal{L}_2 = \eta_2 \frac{\rho c \mathcal{R}}{l_x} \left(T - T_t\right) \tag{66}$$

$$\mathcal{L}_3 = 0 \quad \text{(compatibility condition)} \tag{67}$$

V. Results

In this section the solutions using the GC-NSCBC method are contrasted with solutions computed using the extrapolation technique or with reference simulations available in the literature.

V.A. One-dimensional channel with varying inflow

The first test case is a one-dimensional channel containing an unperturbed mean flow, but then subjected to a sudden increase in the inflow velocity at the left edge. The right edge has an outflow boundary; the bottom and top boundaries are periodic.

The length of the channel is $l_x = 1$ m, and the domain is discretized with 256×32 points. For each boundary, the computational domain is extended by 4 ghost cells as explained in Sec. III. The initial flow velocity is $u_0 = 20$ m/s, while the density is 1.1 kg/m^3 and the static pressure $p_{ref} = 101325$ Pa. Moreover, $\gamma = 1.1$. For simplicity, the flow is considered inviscid, i.e. $\mu = 0$ and $\lambda = 0$. At the inflow boundary, the target inlet velocity is set to $u_t = 2u_0 = 40$ m/s.

For the GC-NSCBC method, the target values for the inflow and outflow conditions are the same as the initial condition, except for the target velocity, which is set to u_t. All the η parameters are set to a value of 2, while $\sigma = 0.25$. No transverse terms are considered here.

For the extrapolation method, the points in the center of the ghost cells are filled with the values of the last point inside the physical domain. For example, if one considers a generic variable Υ at the outflow boundary, $\Upsilon_{Lx+1,\ldots,4} = \Upsilon_{Lx}$. For the inlet boundary, the value of u_t is imposed straight inside the ghost cells for the velocity variable.

The results are depicted in Figure 3. Figures 3.(a)-(b) show the velocity at two different times; Figures 3.(c) and (d) show the density and pressure, respectively, at the latter time when the solution has reached as steady state. In Figure 3.(a), it can be seen that at an early stage of the simulation the velocity very quickly reaches a steady state when the extrapolation technique is employed, whereas the solution with the GC-NSCBC method adjusts more smoothly. However, as shown in Figures 3.(a)-(d), the steady state reached by the flow is wrong when the extrapolation technique is used. This behavior is symptomatic of a ill-posed problem at the boundary condition. It is clear that not only does the velocity not reach the target velocity imposed, but the density and pressure also reach unphysical values. However, with the GC-NSCBC method, all variables reach the expected target values provided at the inflow boundary, and the density and pressure are not affected by the velocity change.

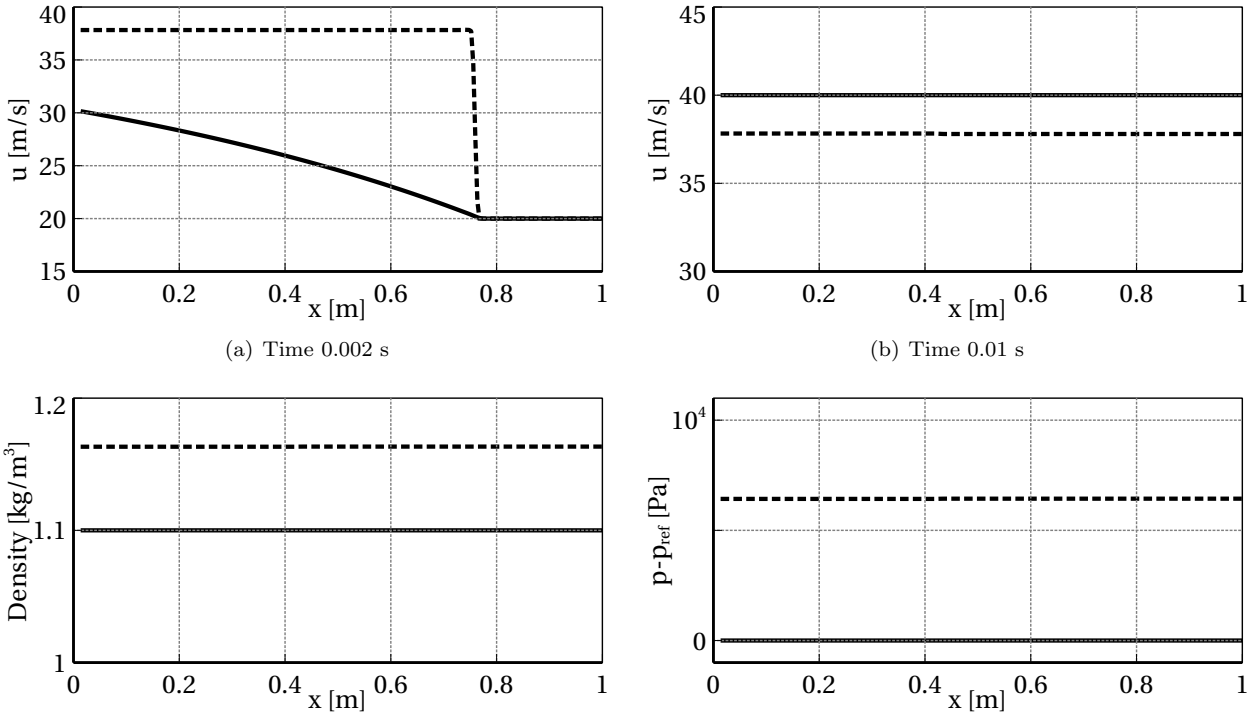

(a) Time 0.002 s

(b) Time 0.01 s

(c) Time 0.01 s

(d) Time 0.01 s

Figure 3. State variables at times 0.002 s and 0.01 s, computed with ghost cells filled with a zeroth-order extrapolation technique (– – –) and the GC-NSCBC method (——).

V.B. Two-dimensional convected vortex leaving a domain

The following test case consists of the convection of a 2D vortex out of a computational domain. This test case has been used frequently in the literature to assess the performance of different formulations of characteristic boundary conditions.[5,9–11] The physical set-up is chosen to replicate Case C in Granet *et al.*[11]

The configuration is a single vortex superimposed on a uniform flow field along the x-direction. The stream function Ψ of the initial vortex is given by

$$\Psi = \Gamma \exp\left(\frac{-r^2}{2R_v^2}\right) + u_0, \tag{68}$$

where $r = \sqrt{(x-x_v)^2 + (y-y_v)^2}$ is the radial distance from the center of the vortex located at $[x_v, y_v]$, while Γ and R_v are the vortex strength and radius, respectively. The velocity field is then defined as

$$u = \frac{\partial \Psi}{\partial x}, \qquad v = \frac{\partial \Psi}{\partial y}. \tag{69}$$

The initial pressure field is expressed as

$$p\,(r) = p_{\text{ref}} \exp\left(-\frac{\gamma}{2}\left(\frac{\Gamma}{cR_v}\right)^2 \exp\left(-\frac{r^2}{R_v^2}\right)\right), \tag{70}$$

and the corresponding density field is given by

$$\rho\left(r\right) = \frac{p\left(r\right)}{\mathcal{R}T_{\text{ref}}}, \tag{71}$$

where T_{ref} is assumed constant.

The computational domain is a square of dimension $L = 0.013$ m and is discretized with 128×128 points. The reference temperature T_{ref} and pressure p_{ref} are set to 300 K and 101325 Pa, respectively. The vortex is located at $[x_v, y_v] = [0, 0]$, and its parameters are set to $\Gamma = 0.11$ m^2/s and $R_v = 0.1L$. The initial flow velocity is $u_0 = 100$ m/s. When the GC-NSCBC method is used, the η parameters for the inflow condition are all set to 1, whereas the σ parameter for the outflow is set to 0.25. For both conditions, the transverse terms are taken into account via the parameter β, which is computed as the average of the Mach number over the boundary considered. Among all of possible definitions of β, it has been demonstrated that this latter choice ensures minimum spurious reflections at boundaries for this particular test case.[11] In this latter reference, Nitrogen is employed in the simulation. In order to replicate the results, the viscosity is accordingly chosen to be $\mu = 2.86 \times 10^{-5}$ kg/(m.s).

Results are depicted in figure 4. The top and bottom rows present the stream-wise velocity contours as well as the normalized pressure field taken at 4 different times, and computed either with the GC-NSCBC method or the zeroth-order extrapolation technique, respectively. The normalized pressure field is defined using the initial pressure at the vortex center and is given by

$$p^* = -p\frac{2R_v^2}{\rho\Gamma^2}, \tag{72}$$

whereas the dimensionless time is defined as $t^* = t/\tau$ with $\tau = L/2u_0$.

Results computed with the GC-NSCBC method are very close to the results published in Granet *et al.*,[11] which are based on a cell-vertex finite volume numerical method that does not require any ghost cells. The vortex begins to interact with the outflow boundary condition at about $t^* = 0.5$ and leaves the domain at $t^* = 1.5$. It is clear that the shape of the vortex is preserved and almost no spurious reflections are sent back into the computational domain. However, when the extrapolation technique is employed to fill the ghost cells, the vortex appears to be sucked through the boundary (see figure 4 at time $t^* = 0.45$) and then distorted. Strong pressure fluctuations are then generated at the boundary and remain in the computational domain as the vortex leaves.

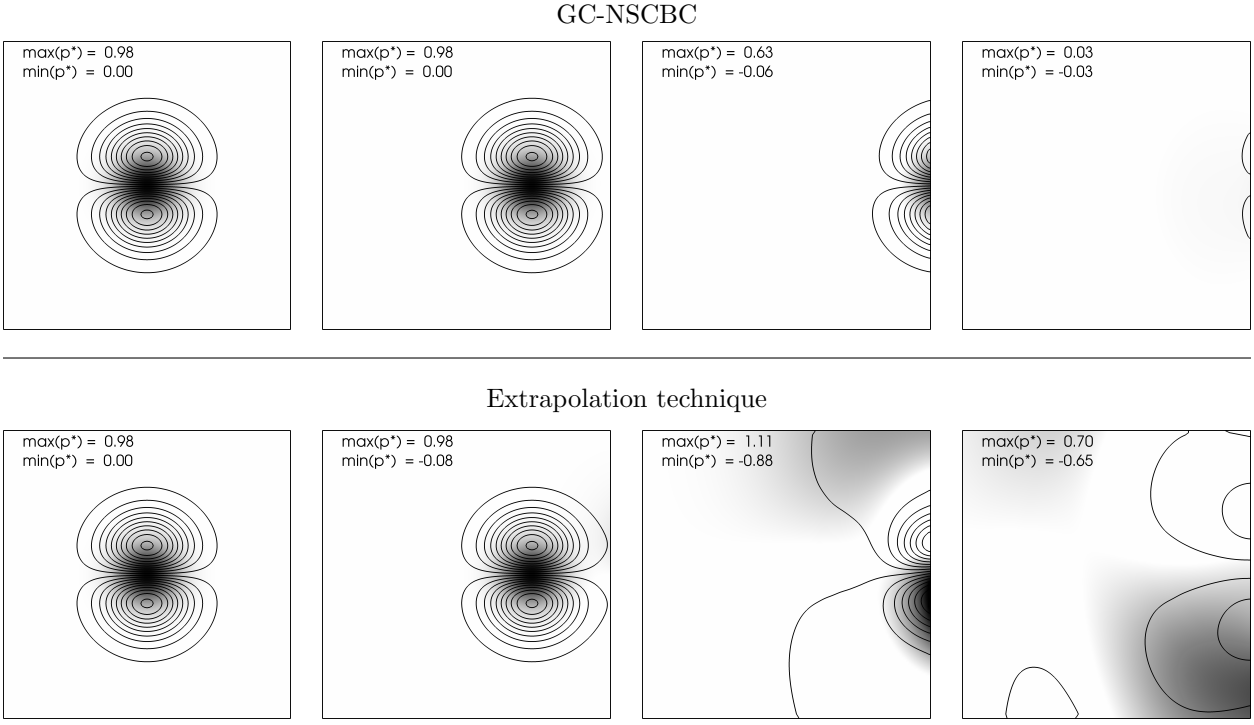

Figure 4. Stream-wise velocity contours and normalized pressure field p^*, at time $t^* = 0, 0.45, 1.12, 1.43$ from left to right.

V.C. Two-dimensional circular pressure wave leaving a square domain

This test case consists of a circular pressure wave generated in the center of a square domain of length $L_x = L_y = L$, and propagating at the sound speed in all directions. All boundaries are set to outflow conditions. This configuration is numerically difficult due to the geometrical mismatch between the circular flow structure and the rectilinear boundary.

The pressure field is initialized as follow:

$$p\left(r\right) = p_{\text{ref}}\left[1 + \delta \exp\left(-\frac{r^2}{2R^2}\right)\right], \tag{73}$$

where δ is the amplitude of the pressure pulse, $r = \sqrt{x^2 + y^2}$ the distance from the center of the computational domain, and R is a characteristic length of the pressure pulse. In the present configuration, $\delta = 0.001$ and $R = 0.05L$ with $L = 0.0013$ m. The domain is discretized with 128×128 points. The background pressure is set to $p_{\text{ref}} = 101300$ Pa. The relative density field is computed from the state equation $\rho\left(r\right) = p\left(r\right)/\left(\mathcal{R}T_{\text{ref}}\right)$ with $T_{\text{ref}} = 300$ K is the uniform temperature. Finally, the viscosity is set to $\mu = 0.001$ kg/(m.s).

When the GC-NSCBC method is employed, the numerical parameters are set to $\sigma = 0.25$ and $\beta = 0.5$. This latter value of β has been reported to give best results for this particular test case.[10] The zeroth-order extrapolation is also tested to provide comparison.

Figures 5.(a) and 5.(b) show the pressure field when the acoustic wave has left the domain, computed with the zeroth-order extrapolation and the GC-NSCBC methods, respectively. When the extrapolation method is employed, spurious inward waves are gradually generated as the physical acoustic wave leaves the domain. As depicted in Figure 5.(a), the combination of physical and spurious acoustic waves leads to a distorted pressure field that features a square shape. As shown in Figure 5.(b), the GC-NSCBC method is able to preserve the circular shape of the acoustic wave. Moreover, no numerical instability appears at corners and the wave leaves the domain smoothly.

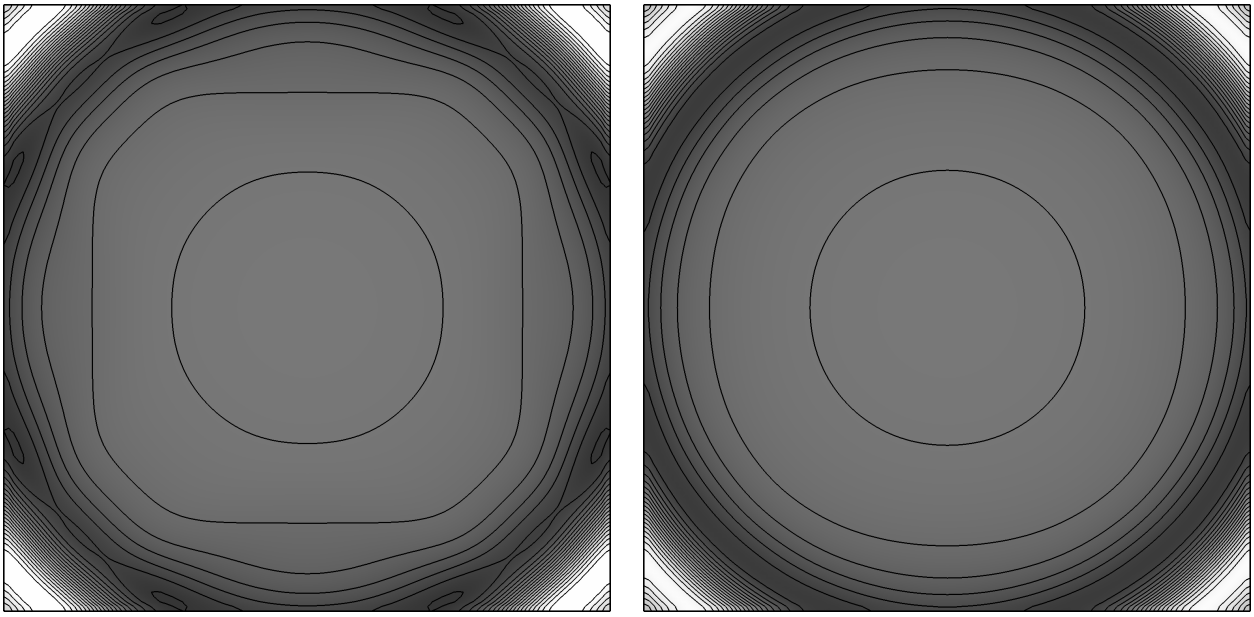

(a) Zeroth-order extrapolation (b) GC-NSCBC

Figure 5. Circular pressure wave leaving a square domain: pressure contours superimposed on top of pressure map.

V.D. Two-dimensional backward-facing step

The behavior of the GC-NSCBC method in the context of a complex configuration is now investigated by simulating the classical backward-facing step test case. The set-up of the configuration is identical to the benchmark simulation provided by Gartling.[25] It consists of a rectangular domain of length $L = 15H$, where H is the height of the domain. An expansion ratio $1/h$ is defined and set to a value of 2. On the left boundary, an inflow velocity is imposed for $h \leqslant y \leqslant 1$ and follows the target parabolic profile $u_t(y) = 24y(0.5 - y)$. For $0 \leqslant y < h$ as well as for the top and bottom boundaries, a no-slip wall condition is imposed. An outflow condition is imposed at the right end of the domain.

The domain is discretized with a grid of 960×64 points. For the inlet condition, all the η parameters are set to a value of 2. For the outflow, $\sigma = 0.25$. For both inflow and outflow, the β parameter is set to the edge-averaged value of the Mach number. The initial solution is a flow at rest with no velocity. The initial density and pressure are set to $\rho_0 = 1.17$ kg/m^3 and $p_0 = 101325$ Pa, respectively. Moreover, $\gamma = 1.4$. Note

that in addition to the velocity profile at the inflow, the target inlet temperature is set to $T_t = p_0/\mathcal{R}\rho_0$. The target outflow pressure is set to $p_t = p_0$ as well. As reported in the reference test case, the Reynolds number is $Re = 800$.

After starting the simulation, the flow enters the domain and reaches a steady state. Note that the Mach number is small ($\max(M) = 0.004$) and due to the CFL restriction, reaching convergence is a fairly long process. The streamlines of the flow are depicted in Figure 7. Note that the right part of the domain has been omitted for clarity. The flow features two recirculation zones, on the lower and upper walls, similar to the reference solution provided by Gartling.[25] Figure 7 presents quantitative comparisons of the $u-$velocity field taken along the $y-$axis at $x = 7$ m. Results computed with the present algorithm (solid line) are very similar to the reference solution (black circles). Moreover, no numerical instabilities have been noticed in the flow and near corners of the domain. This present test case demonstrates that the GC-NSCBC method is able to handle complex flows at boundaries, while a variety of boundary conditions are imposed and coupled at the corners of the domain.

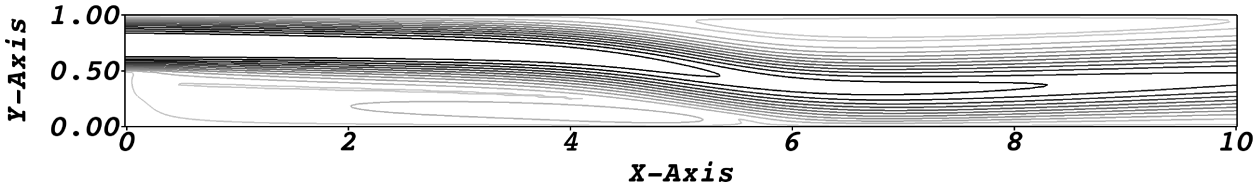

Figure 6. Streamlines of the flow between $x = 0$ and $x = 10$ m.

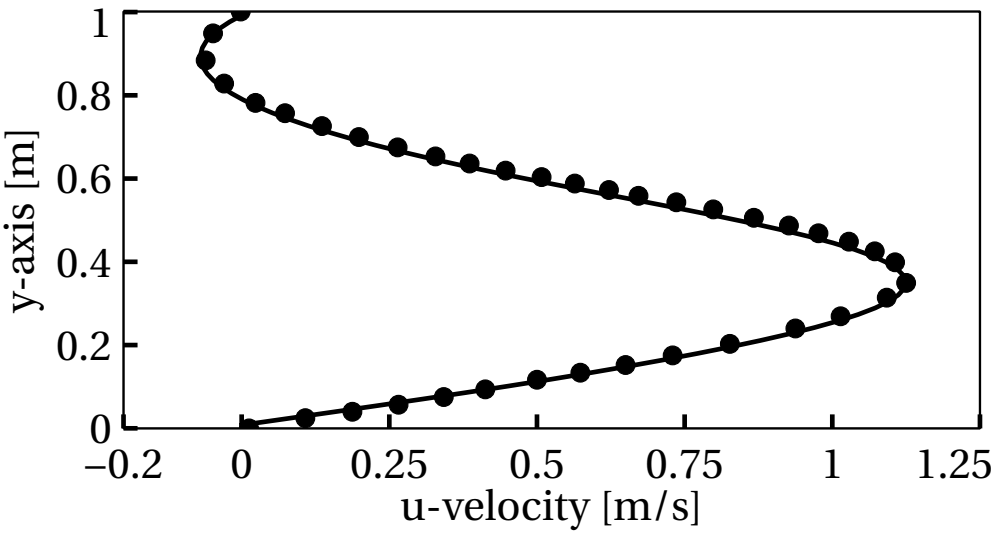

Figure 7. Profile of $u-$velocity along $y-$axis, taken at $x = 7$ m. Solid line (——): present algorithm with GC-NSCBC method. Black circles (•): reference solution.[25]

VI. Conclusions

A new technique based on the NSCBC approach has been presented to derive values for ghost cells that significantly improves the treatment of boundaries over simple extrapolation but retains the ghost cells approach. Comparisons with simulations using extrapolated boundary conditions demonstrate the efficacy of the new approach. The modification of the inlet velocity in a one-dimensional channel demonstrates that with the GC-NSCBC treatment the flow is able to adapt to a sudden change in velocity imposed at an inflow boundary. When the zeroth-order extrapolation technique is employed to fill ghost cells values, the interior flow reaches an unphysical steady state. In a 2D simulation of a convected vortex leaving a square domain, GC-NSCBC treatment of the outflow boundary preserves the shape of the vortex as it leaves the domain, and no spurious reflections are sent back. With the extrapolation technique, the vortex is significantly distorted as it attempts to leave the domain, and an unphysical pressure field is created inside the domain. The coupling of boundary conditions at the corners of the domain is also treated by the GC-NSCBC method. A simulation of a circular pressure wave leaving a square domain demonstrates the ability of the GC-NSCBC method to preserve the ciruclar shape of the wave, while the zeroth-order extrapolation deteriorates the wave that adopt a square shape. Moreover, the simulation of the flow over a backward-facing step is performed to demonstrate the ability of the GC-NSCBC method to impose flow profiles, and to deal with different boundary conditions coupled at corners. Results are successfully compared to a reference solution published in the literature. Overall, the new GC-NSCBC method proposed in the present paper allows the imposition and control of complex boundary conditions with the simplicity of setting values in ghost cells as opposed to requiring specialized discretizations at boundaries. While a particular Godunov procedure has been employed in the present study, it is emphasized that the GC-NSCBC is applicable to a variety of integration strategies and for an arbitrary number of ghost cells. In addition, the method has been presented in two dimensions for conciseness, but extension to three dimensions is straightforward.

Acknowledgments

The authors wish to thank Dr. Andrew Nonaka and Dr. Weiqun Zhang for their help with CASTRO and BoxLib.

The work here was supported by the U.S. Department of Energy, Office of Science, Office of Advanced Scientific Computing Research, Applied Mathematics program under contract number DE-AC02005CH11231.

References

[1]Motheau, E., Nicoud, F., and Poinsot, T., "Mixed acoustic-entropy combustion instabilities in gas turbines," *J. Fluid Mech.* , Vol. 749, 6 2014, pp. 542–576.

[2]Rudy, D. H. and Strikwerda, J. C., "A non-reflecting outflow boundary condition for subsonic Navier Stokes calculations," *J. Comput. Phys.* , Vol. 36, 1980, pp. 55–70.

[3]Thompson, K. W., "Time dependent boundary conditions for hyperbolic systems," *J. Comput. Phys.* , Vol. 68, 1987, pp. 1–24.

[4]Thompson, K. W., "Time dependent boundary conditions for hyperbolic systems II," *J. Comput. Phys.* , Vol. 89, 1990, pp. 439–461.

[5]Poinsot, T. and Lele, S., "Boundary conditions for direct simulations of compressible viscous flows," *J. Comput. Phys.* , Vol. 101, No. 1, 1992, pp. 104–129.

[6]Baum, M., Poinsot, T. J., and Thévenin, D., "Accurate boundary conditions for multicomponent reactive flows," *J. Comput. Phys.* , Vol. 116, 1994, pp. 247–261.

[7]Kim, J. W. and Lee, D. J., "Generalized Characteristic Boundary Conditions for Computational Aeroacoustics," *AIAA Journal* , Vol. 38, 2000, pp. 2040–2049.

[8]Yoo, C., Wang, Y., Trouvé, A., and Im, H., "Characteristic boundary conditions for direct simulations of turbulent counterflow flames," *Combust. Theory and Modelling* , Vol. 9, 2005, pp. 617–646.

[9]Yoo, C. and Im, H., "Characteristic boundary conditions for simulations of compressible reacting flows with multi-dimensional, viscous, and reaction effects," *Combust. Theory and Modelling* , Vol. 11, 2007, pp. 259–286.

[10]Lodato, G., Domingo, P., and Vervisch, L., "Three-dimensional boundary condtions for direct and large-eddy simulation of compressible viscous flow," *J. Comput. Phys.* , Vol. 227, No. 10, 2008, pp. 5105–5143.

[11]Granet, V., Vermorel, O., Leonard, T., Gicquel, L., and Poinsot, T., "Comparison of Nonreflecting Outlet Boundary Conditions for Compressible Solvers on Unstructured Grids," *AIAA Journal* , Vol. 48, No. 10, 2010, pp. 2348–2364.

[12]Huet, M., "One-dimensional characteristic boundary conditions using nonlinear invariants," *J. Comput. Phys.* , Vol. 283, 2015, pp. 312–328.

[13]Jaensch, S., Sovardi, C., and Polifke, W., "On the robust, flexible and consistent implementation of time domain impedance boundary conditions for compressible flow simulations," *J. Comput. Phys.* , Vol. 314, 2016, pp. 145–159.

[14]LeVeque, R. J., *Finite volume methods for hyperbolic problems*, Cambridge texts in applied mathematics, Cambridge University Press, Cambridge, New York, 2002.

[15]Engquist, B. and Majda, A., "Absorbing boundary conditions for the numerical simulation of waves," *Math. Comput.*, Vol. 31, No. 139, 1977, pp. 629–651.

[16]Berenger, J.-P., "A perfectly matched layer for the absorption of electromagnetic waves," *J. Comput. Phys.* , Vol. 114, No. 2, 1994, pp. 185–200.

[17]Karni, S., "Far-Field Filtering Operators for Suppression of Reflection From Artificial Boundaries," *SIAM J. Numer. Anal.* , Vol. 33, No. 3, 1996, pp. 1014–1047.

[18]Gross, A. and Fasel, H. F., "Characteristic ghost cell boundary condition," *AIAA Journal* , Vol. 45, No. 1, 2007, pp. 302–306.

[19]Almgren, A. S., Beckner, V. E., Bell, J. B., Day, M. S., Howell, L. H., Joggerst, C. C., Lijewski, M. J., Nonaka, A., Singer, M., and Zingale, M., "CASTRO: A New Compressible Astrophysical Solver. I. Hydrodynamics and Self-gravity," *Astrophys. J.* , Vol. 715, No. 2, 2010, pp. 1221.

[20]Zhang, W., Almgren, A., Day, M., Nguyen, T., Shalf, J., and Unat, D., "BoxLib with Tiling: An Adaptive Mesh Refinement Software Framework," *J. Sci. Comput.* , Vol. 38, No. 5, 2016, pp. S156–S172.

[21]Bell, J. B. et al., *BoxLib User's Guide.*, 2016, https://ccse.lbl.gov/BoxLib/.

[22]Miller, G. and Colella, P., "A Conservative Three-Dimensional Eulerian Method for Coupled Solid–Fluid Shock Capturing," *J. Comput. Phys.* , Vol. 183, No. 1, 2002, pp. 26–82.

[23]Colella, P. and Sekora, M. D., "A limiter for PPM that preserves accuracy at smooth extrema," *J. Comput. Phys.* , Vol. 227, No. 15, 2008, pp. 7069–7076.

[24]Fosso P., A., Deniau, H., Lamarque, N., and Poinsot, T., "Comparison of outflow boundary conditions for subsonic aeroacoustic simulations," *Int. J. Numer. Meth. Fluids* , Vol. 68, No. 10, 2012, pp. 1207–1233.

[25]Gartling, D. K., "A test problem for outflow boundary conditions—flow over a backward-facing step," *Int. J. Numer. Meth. Fluids* , Vol. 11, No. 7, 1990, pp. 953–967.